Desalination and Water Treatment
www.deswater.com

28 (2011) 328–337
April

1944-3994/1944-3986
doi: 10/5004/dwt.2011.1413

PV cell-driven humidification-dehumidification (H/D) process for brine treatment

Jun-Hong Wang[a], Nai-Yun Gao[a,*], Yang Deng[b], Sheng-Ji Xia[a], Jun-Lian Qiao[a]

[a]*State Key Laboratory of Pollution Control and Resource Reuse, Tongji University, Shanghai 200092, China*
Tel. +86-21-65982691; email: gaonaiyun@sina.com
[b]*Department of Earth and Environmental Studies, Montclair State University, Montclair, New Jersey 07043, USA*

Received 24 November 2009; Accepted 21 February 2011

ABSTRACT

This study was to technically evaluate a solar still desalination system driven by photovoltaic (PV) cells for treatment of a brine wastewater through evaporation (humidification) and subsequent condensation (dehumidification) processes. Based on the solar radiation data in Shanghai, China, solar energy utilization, freshwater production, and salt production were estimated. Results showed that under the identical operating conditions, air forced convection (5.9 $m \cdot s^{-1}$) exhibited a better performance than free convection with the regards toward air humidification and freshwater productions. However, free convection had much higher energy recovery. Our study demonstrated that the new solar still, powered directly and indirectly by solar energy, is an effective and economic desalination process, and it may be very useful in rural communities.

Key words: Solar stills; Brine; Desalination; Humidification; Dehumidification

1. Introduction

Pressure-driven membrane processes (e.g., NF/RO) inevitably produce a large amount of concentrated wastewater effluent (brine) that must be appropriately disposed of, during seawater desalination. Many methods, such as evaporation [1–6] and distillation techniques [7–9], have been studied to treat and reuse the wastewater. Among them, evaporation shows promising results due to both effective treatment of brine and concurrent recovery of salts and other minerals [5,6]. Solar still is an evaporation-based technique [10], in which, seawater located at the bottom of a greenhouse absorbs solar radiation through as its transparent roof cover, and the temperature difference between the heated seawater and its surrounding environment results in seawater evaporation, followed by condensation on the inner side of its inclined roof that introduces the condensed water down to vents [11]. Solar stills has been one of the most valuable fresh water supplies due to its simple configuration, easy operation, and low operation cost [12–24]. Particularly, such a desalination technology is very attractive for community water supply in rural areas and remote villages [13].

To date, all the studies relevant to solar still have been focused primarily on two categories: flat-plate collectors and concentrators, both of which can enhance evaporation. For example, Schwarzer et al. [20] reported a productivity of 25 $l \cdot d^{-1} \cdot m^2$ achieved by using a solar still system with multi-effect desalination connected to solar collectors [20]. Also, seawater heated by the latent heat of vapor released increased the solar utilization efficiency [20]. Voropoulos et al. [21] used a solar still combined with a hot water tank that stored the solar energy to guarantee a 24-h continuous fresh water supply. Although these studies improved the performances of solar stills, to some degrees, the fresh water production rate significantly changed with a varying daily solar radiation.

The objective of this study is to evaluate the performance of a solar photovoltaic (PV) cell-driven solar still

*Corresponding author.

system, developed from a seawater desalination solar still system, to in treatment of concentrated brine produced from a pressure-driven membrane desalination process.

2. Experimental

2.1. Design concept of solar still system for brine disposal

The design concept of solar still system for brine treatment is shown in Fig. 1. The system is composed of two chambers: evaporation room and condensation room. Two energy sources provide the heat required for water evaporation in the evaporation room. The primary source is solar PV cells, and the auxiliary source is the direct solar irradiation through the transparent roof cover. The solar PV cells not only supply the energy through heater at the bottom of the evaporation room in the daytime, but also solely support evaporation over nights to ensure incessant and reliable fresh water production using the energy stored in batteries in the daytime. As a result of water evaporation, solid salts are formed at the bottom of the brine. Once the humidified air in the evaporation room enters the condensation room, the vapor is condensed by the condensation tubes filled with flowing raw seawater. Finally, the condensed fresh water is collected into a freshwater storage vessel beneath the condensation tubes.

2.2. Weather

All the experiments were conducted in Shanghai, China. The local weather conditions were provided by the Baoshan station in the Shanghai climate center (station #: 58362; latitude: 31.24°; longitude: 121.29°; and elevation relative to the sea level: 6.0 m). Fig. 2 shows a plot of the average annual daily global radiation and time in Shanghai, China during 1991–2007. The data in the plot was fitted using linear regression. As seen, the average annual daily global radiation was almost constant over the entire studied period.

The average annual daily global radiation from 1991 to 2007 was 12.48 $MJ{\cdot}m^{-2}{\cdot}d^{-1}$. Other local weather information in the same period included: the average annual daily atmosphere temperature = 17.0°C; and the average annual daily relative humidity = 73%.

2.3. Solar energy utilization in the solar still system

To simplify the computation, sunlight from the transparent roof cover was ignored, and any heat loss in the system is neglected. PV is the sole energy source to power the desalination, and provides an effective solar energy as follows:

$$Q_{sun} = \eta_{cell} A_{cell} G \tag{1}$$

where, η_{cell}, the PV cell's photoelectric conversion coefficient; A_{cell}, the solar cell area; and G, the average annual daily global radiation. If there is no heat loss during the heat and mass transfer processes, the total energy from the solar cells can be divided into two sections: Q_{evap} used for water evaporation, and Q_{heat} used to heat the water:

$$Q_{sun} = Q_{evap} + Q_{heat} \tag{2}$$

$$Q_{evap} = m_{evap}\gamma_1 = m_{air}(x_{h,1} - x_{c,0})\gamma_1 \tag{3}$$

$$Q_{heat} = m_{air}\overline{C}_{p,air}\Delta t + m_{air}(x_{h,1} - x_{c,0}) \times \overline{C}_{p,water}\Delta t + m_{air}x_{c,0}(h_{evapor,1} - h_{evapor,0}) \tag{4}$$

where, m, C_p, x, h_e are the mass flow rate, specific heat and absolute humidity of air and enthalpy, respectively;

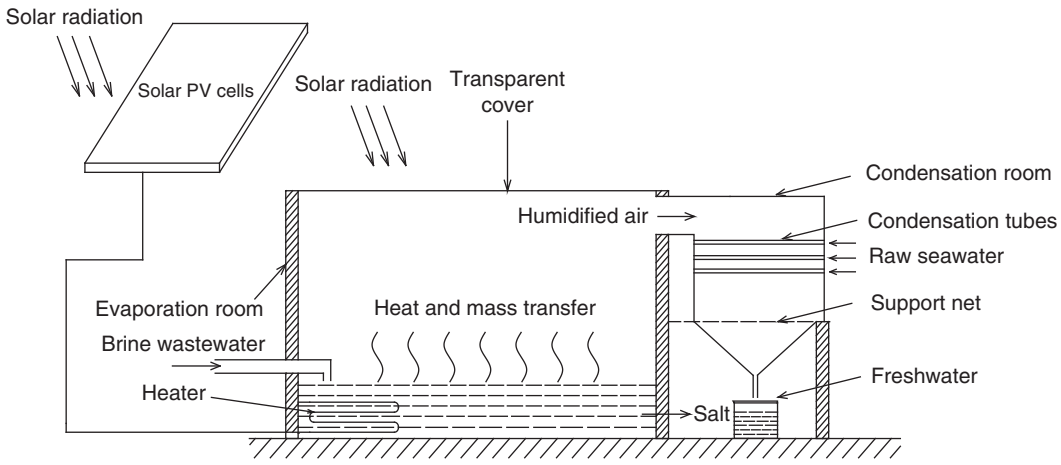

Fig. 1. Design concept of a solar still system for brine disposal, freshwater recovery, and salt formation.

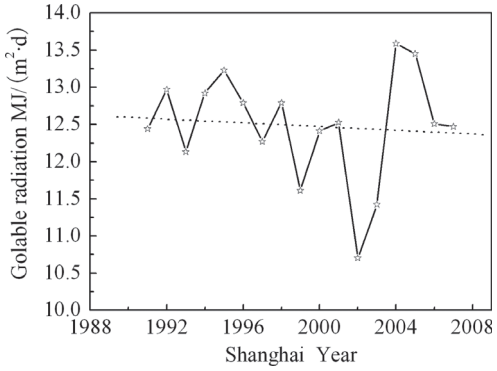

Fig. 2. Plot of the average annual daily global radiation and time at the Baoshan station in Shanghai, China.

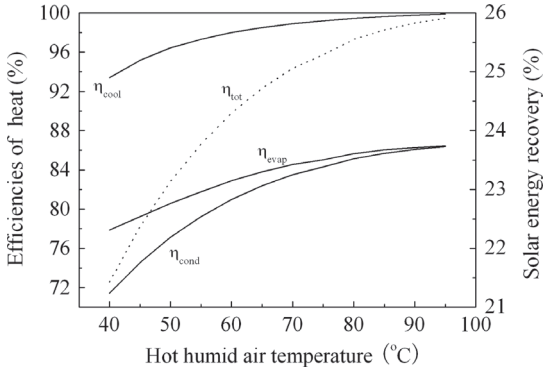

Fig. 3. Variation curves of solar efficiencies with operation hot humid air temperature ($t_0 = t_2 = 17$°C, $\Phi_0 = 73\%$, $\Phi_1 = 100\%$; the curves of η_{cool}, η_{evap}, and η_{cond} for the primary y axis, and the η_{tot} curve for the secondary y axis).

subscripts 0, 1, h, c, and *air* indicate the initial temperature, final temperature, hot moist air, cold humid air, and dry air, respectively; $m_{air}C_p\Delta t$ represents the energy to heat dry air; $m_{air}(x_{h,1}–x_{c,0})C_{p,water}\Delta t$ means the heat energy to heat the vapor from the initial to the final state; and $m_{air}x_{c,0}(h_{evapor,1}–h_{evapor,0})$ is the energy to heat the vapor in cold air.

On the other side, the solar energy absorbed can be written as follows:

$$Q_{sun} = m_{air}h_{eh,1} - m_{air}\left(x_{h,1} - x_{c,0}\right)h_{ewater,0} - m_{air}h_{ec,0} \tag{5}$$

where, $m_{air}h_{eh,1}$ is the hot humid air heat energy; $m_{air}(x_{h,1}–x_{c,0})h_{ewater,0}$ means the heat of evaporated water at t_0; and $m_{air}h_{ec,0}$ is the heat for cold humid air at the initial system state. Once entering the condensation chamber, the hot humid air was cooled down, and the temperature was decreased to t_2. To condense the hot humid air, the air was back to a saturated state, and its lowest temperature was same as that of the initial cooling water at the entrance. Based on the double-film theory, we assumed no vapor condensation during the mass transfer process through the air layer. Therefore, the latent heat energy released for condensate is given as follows:

$$Q_{cond} = m_{cond}\gamma_1 = m_{air}\left(x_{h,1} - x_{c,2s}\right)\gamma_1 \tag{6}$$

where, subscripts *cond* and *s* stand for condensation and saturated states, respectively.

Based on the law of energy conservation, the total energy released for condensation, including sensible heat and latent heat, can be expressed as:

$$Q_{cool} = m_{air}h_{eh,1} - m_{air}h_{ec,2s} - m_{air}(x_{h,1} - x_{c,2s})h_{ewater,2} \tag{7}$$

where, $m_{air}h_{ec,2s}$ is the cold saturated air after condensation, and $m_{air}(x_{h,1}–x_{c,2s})h_{ewater,2}$ is the heat of condensate at t_2.

The solar utilization efficiencies for evaporation, and condensation and cooling, can be represented by the flowing equations, respectively:

$$\eta_{evap} = Q_{evap}/Q_{sun} \tag{8}$$

$$\eta_{cond} = Q_{cond}/Q_{sun} \tag{9}$$

$$\eta_{cool} = Q_{cool}/Q_{sun} \tag{10}$$

And the overall solar energy recovery of the system is as follows:

$$\eta_{tot} = \eta_{cell} \times \eta_{cond} \tag{11}$$

In the evaporation room, the initial temperature t_0 was 17.0°C, the initial relative humidity Φ_0 was 73%, the final hot air was humidified to a saturated state (Φ_1=100%), and the cooling water temperature t_2 was 17.0°C. Moreover, we assumed that the photoelectric conversion efficiency η_{cell} was 0.3 [25]. Under such conditions, the plots of the solar utilization efficiencies during different steps (evaporation, condensation, and cooling), as well as the overall solar energy recovery with of the operating hot humid air temperature are shown Fig. 3. As seen, all the efficiencies increased with the increasing hot humid air temperature.

After combination of the above equations, the quantities of evaporated water and condensate can be determined by the flowing equations, respectively:

$$m_{evap} = \frac{\eta_{evap}Q_{sun}}{\gamma_1} = \frac{(x_{h,1} - x_{c,0})\eta_{cell}A_{cell}G}{h_{eh,1} - (x_{h,1} - x_{c,0})h_{ewater,0} - h_{ec,0}} \tag{12}$$

$$m_{cond} = \frac{\eta_{cond} Q_{sun}}{\gamma_1} = \frac{(x_{h,1} - x_{c,2s})\eta_{cell} A_{cell} G}{h_{eh,1} - (x_{h,1} - x_{c,0}) h_{ewater,0} - h_{ec,0}} \quad (13)$$

With the progress of evaporation, salt crystals gradually deposited from brine waste. The average salt quantity can be estimated in Eq. (14):

$$\bar{m}_{salt} = m_{evap} C_{brine} \quad (14)$$

where, C_{brine} is the brine concentration. Due to the dilution of the Yangtze River, the seawater salinity near Shanghai typically fluctuated from 0.25% to 1.3%. If the saline concentration of raw seawater was 1%, the water recovery of membrane desalination process was 50%, and two RO units were used, C_{brine} was calculated as 4%.

Table 1
Productivity of system at different operation temperatures of hot humid air

t_0 (°C)	m_{evap} (kg·m^{-2}·d^{-1})	m_{cond} (kg·m^{-2}·d^{-1})	m_{salt} (kg·m^{-2}·d^{-1})
40	1.214	1.114	0.049
45	1.241	1.168	0.050
50	1.268	1.214	0.051
55	1.294	1.254	0.052
60	1.318	1.287	0.053
65	1.339	1.316	0.054
70	1.358	1.341	0.055
75	1.375	1.363	0.056
80	1.390	1.382	0.056
85	1.403	1.398	0.057
90	1.415	1.412	0.057

Table 1 shows the estimated production rates of evaporated water, condensate and salt at different hot humid air temperatures in 1 m^2 solar PV cells area.

2.4. Experiments

The brine used in this study was a simulated one with 30 g/l NaCl. Fig. 4 shows the schematic diagram of our experimental setup that was mainly composed of an evaporation unit, a condensation unit and a data detective part. The evaporation unit included an evaporation chamber, a temperature sensor, a control panel, and an auxiliary heater coil (3,500 W). The condensation unit consisted of a condensation chamber, three horizontal tubes, a freshwater measuring cylinder, a water separator with flow meters, a cooling water tank, and a pressure pump. The data detective part for dry and wet-bulb temperatures was composed of a PJ-7115 Pt conditioning plate, a PCI-7422 A/D (Beijing Macro Extension Control Technology Co., Ltd.), a desktop, data cables, and a Pt resistance.

Brine was first heated by heater coil in the evaporation chamber, and its temperature was maintained at a desirable level by the temperature control panel and sensor. Meanwhile, the air in the evaporation room, after being heated and humidified by the brine, would enter the condensation room through the bridging channel. A fan (5.9 m·s^{-1} wind speed, AF 2155 HS (B) L, Shenzhen Lianxiang Electrical-machines Co., Ltd.) was installed in the channel to increase the air flow velocity and enhance the mass transfer. Once the vapor contacted the cooling tubes in the condensation chamber, the flowing cooling water in the horizontal tubes adsorbed heat from the hot humidified air, and resulted in the formation of condensed water on the tube surface. With the accumulation of condensed water on the tubes, water eventually

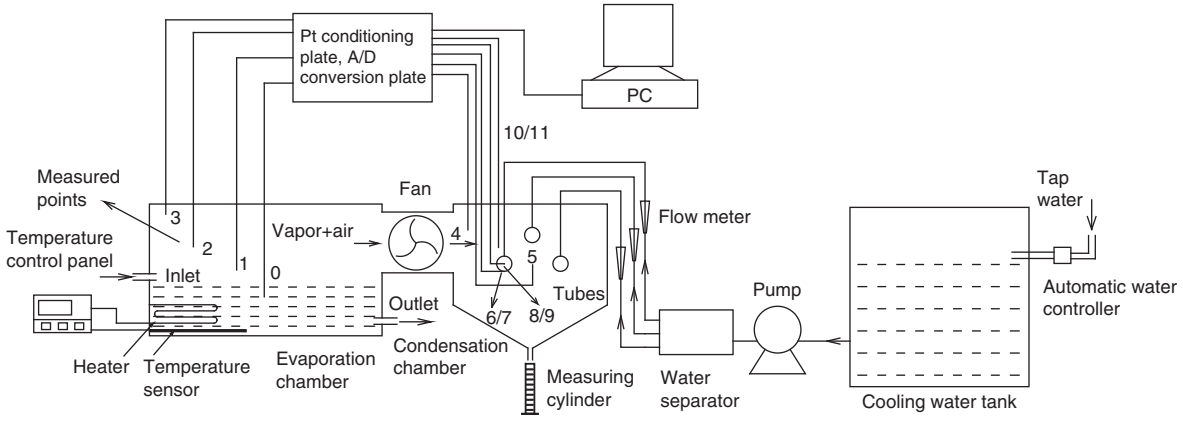

Fig. 4. Schematic diagram of experimental setup.

dropped into the measuring cylinder at the bottom. The evaporation chamber was a sealed 500 × 400 × 400 mm polyvinyl chloride (PVC) box with a 10mm-thickness. The condensation chamber was a 400 mm (diameter) × 500 mm (height) cylinder with a bottom inclined at an angle of $\pi/6$. In the condensation chamber, three 15 mm (diameter) × 1.5mm (thickness) smooth red copper tubes were horizontally arranged in an equilateral triangle with a 120 mm space between any two. Both of the chambers were totally packed by sponges serving as a heat insulting material. Moreover, the water separator split tap water stored in the cooling water tank via a pump into three cooling flows. The three pipes were connected with the cooling system in the condensation chamber.

Temperatures of this system were real-time monitored at different monitor points. At each monitor point, there was a Pt resistance probe made of Pt100 with a temperature range of 0°C ~ 100°C. The signal transmission system could input the resistance signals into PJ-7115 Pt adjusting board. The signals were then translated to into voltage signals through PCI-7422 A/D board, and finally transferred to a temperature output from a desktop. All the monitor points, except points 6 and 7, outputted dry and wet-bulb temperatures. The points 6 and 7 outputted tube temperatures. In the evaporation chamber, Pt resistance was switched at points 0, 1, 2, or 3 as shown in Fig .4. The point 0 was located in brine, and the points 1, 2 and 3 were located in 2, 20 and 35cm above the brine surface, respectively. Monitor points in the condensation chamber were fixed on the tube surface (the entrance points, exit 6 and 7), cooling water body (the entrance points, exit 8 and 9) and hot humidified air body (the entrance of condensation room 4, and the middle point of condensation tube 5), and upper air tube surface (the entrance, exit 10 and 11).

3. Results and discussions

3.1. The transient-state condensation

Fig. 5a and 5b show the plots of temperatures and relative humidity for air with time in the evaporation chamber under the forced convection (air flow rate = 5.9 m·s^{-1}), respectively. As shown in Fig. 5a, the brine temperature approached a steady state temperatures at 30 min (t_0 = 45°C). And the air temperatures in the middle and upper evaporation chambers (t_2 and t_3) were almost overlapped, slightly higher than that on the brine surface (t_1). As seen in Fig. 5b, air on the brine surface and at the upper chamber was humidified to a saturated steady-state after 30 min. However, the middle air chamber was at an unsaturated state during the study period.

The freshwater production over time in the condensation chamber is shown in Fig. 6a. As seen, a quasi-steady rate of water production was achieved at 50 min when the temperature reached a steady-state. Fig. 6b shows the plot of the freshwater production rate and time under free convection with a steady-state brine temperature of 50°C. As seen, brine temperature reached the steady state at 50 min. Of interest, the fresh water collection rate increased from 0.008 to 0.015 g·s^{-1} with the increasing time from 50 to 55 min, and then decreased to 0.008 at 80 min. After 80 min, the production rate almost stabilized at 0.008 g·s^{-1}.

3.2. Effects of free and forced convections

Table 2 shows the effects of free and forced convections on the system performance. Apparently, the forced convection could generate a much higher freshwater production rate (0.034 g·s^{-1}) than the free convection (0.008 g·s^{-1}). As a result of a high air flow rate under the forced convection (air flow rate = 5.9 m·s^{-1}), the

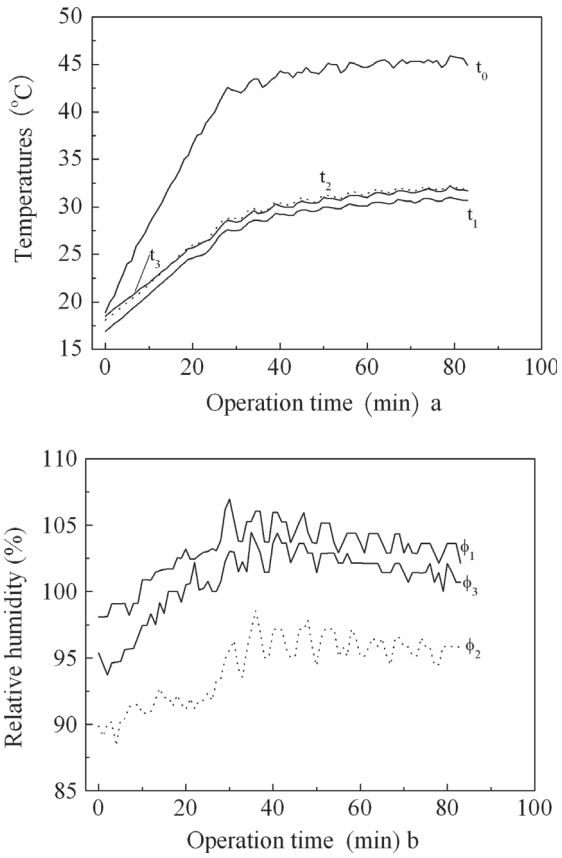

Fig. 5. Temperatures and relative humidity vs. operation time under the forced convection in the evaporation chamber. a) temperatures vs. operation time; and b) relative humidity vs. operation time (subscripts 0, 1, 2, 3 represent brine, air on the brine surface, air in the middle evaporation chamber, air at the upper evaporation chamber, respectively)

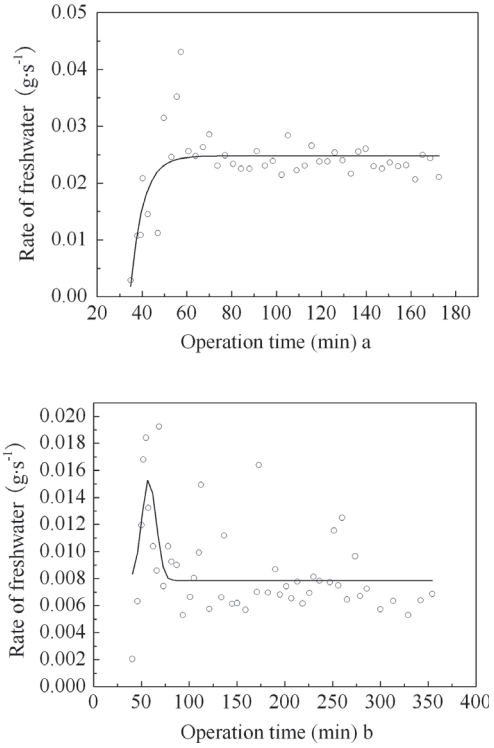

Fig. 6. Production/collection rates of freshwater vs. operation time under the forced convection in the condensation and evaporation chambers. a) production rate vs. operation time in the condensation chamber (brine temperature = 45°C, rate of cooling water = 1.0 m·s^{-1}, and air flow rate = 5.9 m·s^{-1}); and b) Curve of collecting rate of freshwater vs. operation time in the evaporation chamber (brine temperature = 50°C, and rate of cooling water was 0.5 m·s^{-1})

humidified air more rapidly moved to the condensation chamber for condensation. Besides, the air temperature in the middle section of the evaporation chamber was the higher that those on the brine surface and in the upper chamber. In contrast, under a free convection condition, in the highest temperature was t_3.

3.3. Freshwater productions

When vapor crossed the air film, located between the air phase and the condensate film on the cooling water tubes, the vapor temperature could dropped to the temperature of the condensate film. No vapor condensation occurred during the process. Subsequently, the latent heat released by the vapor was immediately absorbed by cooling water, assuming that the heat was not lost. Thus, the condensing rate of vapor can be calculated formulas as follows:

$$m_{cond} = Q_{cwater}/\gamma \quad (15)$$

$$Q_{cwater} = m_{cwater} C_{p,cwater} \Delta t_{cwater} \quad (16)$$

where γ is the latent heat energy released, and Q_{cwater} is the energy absorbed by cooling water. Because there might be a time lag between vapor condensation and freshwater collection, a dropping recovery coefficient was used to define the ratio of the condensation rate and freshwater collection rate.

$$\omega = m_{coll}/m_{cond} \quad (17)$$

Fig. 7a and b show curves of condensation rates, freshwater collection rates and dropping recovery coefficients at different operation brine temperatures under the free and forced convections, respectively. As seen, at any particular brine temperature, the forced convection achieved a higher condensation rate, freshwater collection rate, and coefficient dropping recovery than the free convection. Also, under a free or forced condition, the condensation rate was much higher than the collection rate. For example, with the increasing temperature from 55 to 80°C, the condensation rate was increased from 0.53 to 0.96 g·s^{-1}, but the freshwater collection rate only went up from 0.014 to 0.063 g·s^{-1}, at a free convection.

3.4. Energy recovery at a steady-state operation

Initially, a large amount of energy was required to heat the brine to a desirable temperature. Thereafter, the energy required to maintain the temperature would be reduced. The coefficient of heat energy recovery in the total system can be defined by:

$$\eta_{cwater} = Q_{cwater}/Q_{heater} \quad (18)$$

Table 2
The effects of free and forced convections on system operation steady-state

	t_0 (°C)	t_1 (°C)	t_2 (°C)	t_3 (°C)	Φ_1 (%)	Φ_2 (%)	Φ_3 (%)	x_3 (g·kgair^{-1})	m_{coll} (g·s^{-1})
Free convection	50.0	41.1	42.2	43.2	101.22	97.62	94.76	56.09	0.008
Forced convection	51.5	32.0	33.3	33.1	106.41	97.28	100.00	33.11	0.034

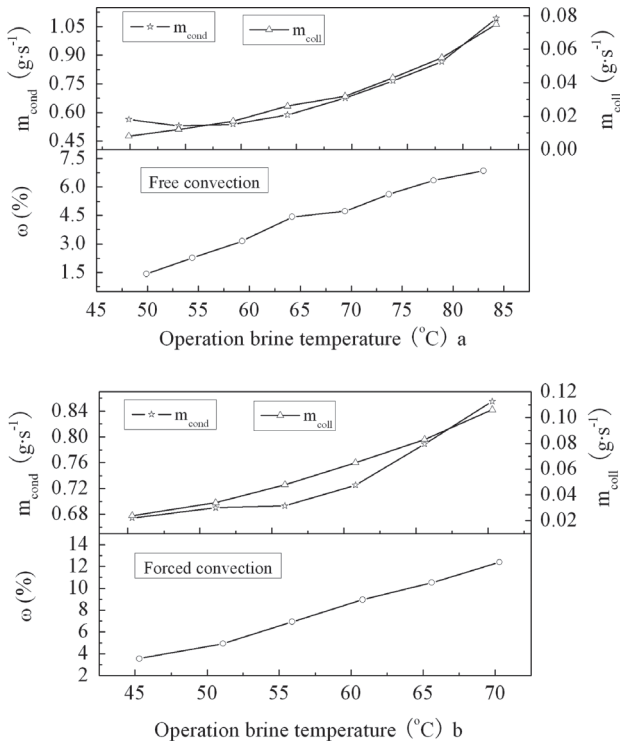

Fig. 7. Freshwater condensation rates, collection rates and dropping recovery coefficients at different operation brine temperatures (cooling water flow rate was 0.5 m·s^{-1}). a) under free convection; and b) under forced convection.

where Q_{heater} is energy provided from the heater, as computed in Eq. (5). To determine Q_{heater}, we assumed:

1. Energy offered by the heater was only consumed to heat and humidify air.
2. Water evaporated from the brine could not withdraw any energy from the brine.
3. Air flow rates were uniformly distributed in the system.

Where, the air flux can be determined in the flowing equations:

$$\bar{m}_{air} = \rho_{air} A_{exit} u_3$$

$$E_k = \Delta P \times u_3 \times A_{exit} = \frac{1}{2} \dot{m}_{air} u_3^2$$

$$u_3 = \left[2\Delta P / \rho_{air,3} \right]^{1/2} \tag{19}$$

where u_3 is the air flow rate in the exit, E_k is the kinetic energy of the heated air, ΔP is the air pressure difference in the evaporation chamber, and A_{exit} is the exit area in the evaporation chamber. ΔP can be integrated by:

$$\Delta P = \int_0^h \left[\rho_1 - \rho(y) \right] dy \tag{20}$$

Generally, the volume expansion coefficient β is defined to characterize the variation of air density caused by temperature difference:

$$\beta = -\frac{1}{\rho} \frac{\partial \rho}{\partial T}\bigg|_P \tag{21}$$

Assuming that air is an ideal gas in the chamber, then $\beta = 1/T$. Ignoring the change of pressure, it can be integrated by:

$$\rho - \rho_1 = -\int_{T_1}^{T} \rho \beta dT = -\overline{\rho\beta}(T - T_1) \tag{22}$$

Because the air temperature difference in the chamber was very low, ρ and β can be calculated using the average air temperature in the chamber. Under the free convection, air temperature in the evaporation chamber linearly increased with the chamber height. Thus, air temperature in the chamber can be represented by:

$$T(y) - T_1 = \frac{h - y}{h} (T_3 - T_1) \tag{23}$$

where h is the height from the brine surface. Based on the equations above, air flow rate is deduced by:

$$u_3 = \left[\frac{\overline{\rho\beta}}{\rho_{air,3}} gh(T_3 - T_1) \right]^{1/2} \tag{24}$$

Fig. 8 shows the heat energy recovery of the total system at different operation brine temperatures. Under

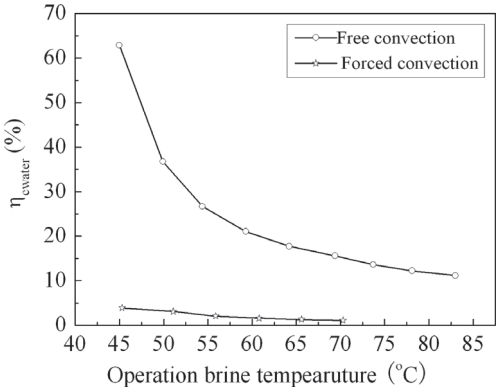

Fig. 8. Curves of heat energy recovery at different operation brine temperatures under free and forced convections (cooling water rate was 0.5 m·s^{-1}).

Table 3a
Characteristics parameters of the PV cell-driven solar still under air free convection at different brine temperatures

t_0 °C	m_{evap} (kg·m^{-2}·d^{-1})	$m_{cond,tube}$ (×10^3 kg·m^{-2}·d^{-1})	$m_{cond,PV}$ (kg·m^{-2}·d^{-1})	A_{cond} (×10^{-3} m^2)	A_{PV} (m^2)	W_{batt} (J·s^{-1})
49.9	109.341	229.271	1.213	2.981	40.070	1736.386
54.4	146.292	215.844	1.242	4.236	36.843	1596.527
59.3	194.152	219.212	1.271	5.536	36.564	1584.443
64.2	259.885	239.144	1.304	6.792	38.879	1684.767
69.4	350.254	275.616	1.333	7.943	43.834	1899.469
73.7	464.847	311.709	1.356	9.321	48.733	2111.775
78.1	607.35	352.919	1.394	10.756	53.672	2325.789
83.0	841.217	445.502	1.394	11.802	67.752	2935.924

Table 3b
Characteristics parameters of the PV cell-driven solar still under air forced convection at different brine temperatures

t_0 °C	m_{evap} (×10^3 kg·m^{-2}·d^{-1})	m_{cond} (×10^3 kg·m^{-2}·d^{-1})	$m_{cond,PV}$ (kg·m^{-2}·d^{-1})	A_{cond} (×10^{-3} m^2)	A_{PV} (m^2)	W_{batt} (J·s^{-1})
45.3	7.332	274.888	1.158	26.674	51.179	2217.753
51.1	9.630	281.197	1.172	34.245	51.719	2241.156
55.9	15.222	282.448	1.214	53.893	50.178	2174.367
60.8	21.557	295.592	1.251	72.928	50.946	2207.674
65.6	29.895	321.531	1.289	92.976	53.736	2328.549
70.3	37.962	348.330	1.315	108.984	57.011	2470.460

an air free convection, the system's heat energy recovery was decreased from 63% to 12% with the increasing temperature from 45 to 80°C. In contrast, under the forced convection, the heat energy recovery was decreased from 4% to 1% with the increasing temperature from 45 to 70°C. The difference in the both heat energy recovery trends is because the condensing areas was not increased correspondingly with the increasing temperature and heat/mass transfer under the forced convection. Consequently most of the vapor could not be condensed in a short time.

3.5. Characteristics parameters of PV cell-driven under full condensation

Table 3a and 3b show the amount of evaporated water per 1m^2 evaporation area, amount of condensate per 1m^2 condensation area, and amount of condensate per 1m^2 solar PV cell, condensing tube area needed per 1m^2 evaporation area for complete condensation, the required PV cells area (for Shanghai, China), and energy storage of backup batteries under free and forced convections. As shown, a high condensing area could achieve a high freshwater production. Typically, forced convection had a much larger condensing area, a higher freshwater production rate, and a higher freshwater production per unit area of solar PV cell than free convection at a specific temperature. Moreover, the PV cells areas required to store energy to backup batteries were different at the different brine temperatures. Under the free and forced convection experiments, the smallest areas were observed at the brine temperatures of 59.3°C and 55.9°C respectively.

The curves of heat energy recovery absorbed by cooling water under free and forced convections are shown in Fig. 9. As seen, at any particular brine temperature, free convection had a higher energy recovery than forced convection. Generally, the energy recovery increased with the increasing brine temperature. The exception is that the energy recovery deceased from

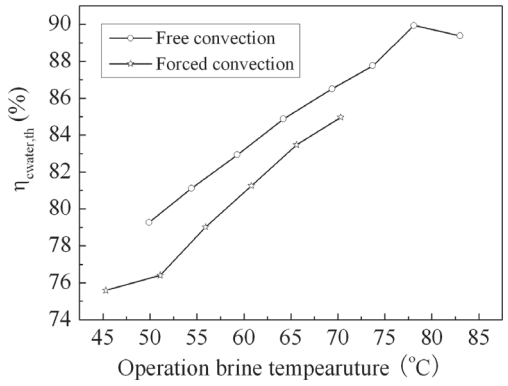

Fig. 9. Curves of heat energy recovery at different operation brine temperatures under the free and forced convection conditions (cooling water rate was 0.5 m·s^{-1}).

89.94% to 89.38% when the brine temperature increased from 78°C to 83°C under free convection. The possible reason is that the condensate film was too thick at 83°C, so that the heat energy through the film was reduced.

4. Conclusions

Our results showed promising results in treatment of brine by a PV cell-driven solar still. With the power provided directly and indirectly from the solar energy, the solar still could be independently and continuously operated. This study demonstrated that the new solar still system may be a better option for disposal of brine, and even for seawater desalination, in rural communities.

Symbols

A	—	Surface area, (m^2)
C_p	—	Specific heat, ($kJ \cdot kg^{-1} \cdot °C^{-1}$)
E_k	—	Kinetic energy of air, ($kJ \cdot s^{-1}$)
g	—	Constant of gravity acceleration, ($9.80 m \cdot s^{-2}$)
G	—	Solar global radiation, ($MJ \cdot m^{-2} \cdot d^{-1}$)
h	—	The height of evaporation chamber, (m)
x	—	Absolute humidity ratio of air, ($kg \cdot kg^{-1}$ dry air)
h_e	—	Enthalpy, ($kJ \cdot kg^{-1}$)
m	—	Mass productivity, ($kg \cdot m^{-2} \cdot d^{-1}$), mass flow rate of air, ($kg \cdot s^{-1}$)
P	—	Pressure of air, (Pa)
Q	—	Heat energy, ($kJ \cdot s^{-1}$)
T	—	Temperature, (K)
t	—	Temperature, (°C)
u	—	Air flow velocity, ($m \cdot s^{-1}$)
W	—	Energy storage of backup batteries, ($J \cdot s^{-1}$)

Greek

β	—	Volume expansion coefficient
γ	—	Heat of vaporization of water, ($kJ \cdot kg^{-1}$)
η	—	Energy conversion coefficient, or solar utilization efficiency
ρ	—	Density, ($kg \cdot m^{-3}$)
Φ	—	Relative humidity of air, (%)
ω	—	Coefficient of dropping recovery

Subcripts

0	—	Brine water
1	—	Air on brine water surface
2	—	Air in the middle of evaporation chamber
3	—	Air at the top of evaporation chamber
air	—	Cold dry air
batt	—	The backup batteries
c	—	Cold humid air
cell	—	Solar PV cells
coll	—	Collection of freshwater
cond	—	Condensate
cool	—	The total processes of condensation including process of air releasing heat
cwater	—	Cooling water
evap	—	The process of evaporation
h	—	Hot humid air
s	—	Saturated state
sun	—	The effective solar energy transferred by PV cells

References

[1] H. Ettouney, Design and analysis of H/D desalination process, Desalination, 183(1–3) (2005) 341–352.
[2] M.B. Amara, I. Houcine, A. Guizani and M. Maâlej, Theoretical and experimental study of a humidifier used in seawater desalination process, Desalination, 168 (2004) 1–12.
[3] M.A. Younis, M.A. Darwish and F. Juwayhel, Experimental and theoretical study of a humidification-dehumidification desalting system, Desalination, 94(1) (1993) 11–24.
[4] L. Awerbuch and M.C. Weekes, Disposal of concentrates from Brackish water desalting plants by means of evaporation technology, Desalination, 78(1) (1990) 71–76.
[5] M. Ahmed, W.H. Shayya, D. Hoey and J. Al-Handaly, Brine disposal from reverse osmosis desalination plants in Oman and the United Arab Emirates, Desalination, 133(2) (2001) 135–147.
[6] J. Truesdall, M. Mickley and R. Hamilton, Survey of membrane drinking water plant disposal methods, Desalination, 102(1–3) (1995) 93–105.
[7] G.N. Tiwari and A.K. Singh, Solar Distillation (2000), Available in: http://www.desware.net.
[8] G.N. Tiwari, H.N. Singh and R. Tripathi, Present status of solar distillation, Sol. Energy, 75(5) (2003) 367–373.
[9] H. Lu, J.C. Walton and A.H.P. Swift, Desalination coupled with salinity-gradient solar ponds, Desalination, 136(1–3) (2001) 13–23.
[10] B.V. der Bruggen and C. Vandecasteele, Distillation vs. membrane filtration: overview of process evolutions in seawater desalination, Desalination, 143(3) (2002) 207–218.
[11] Bachir Bouchekima, A solar desalination plant for domestic water needs in arid areas of South Algeria, Desalination, 153(1– 3) (2003) 65–69.
[12] M. Reali and G. Modica, Solar stills made with tubes for seawater desalting, Desalination, 220(1–3) (2008) 626–632.
[13] N. Nagai, Solar desalination in desert areas, J. Heat Transfer Soc. Japan, 43 (2004) 13.
[14] K.V. Kumar and R.K. Bai, Performance study on solar still with enhanced condensation, Desalination, 230(1–3) (2008) 51–61.
[15] H. Kunze, A new approach to solar desalination for small- and medium-size use in remote areas, Desalination, 139(1–3) (2001) 35–41.
[16] S. Al-Kharabsheh and D.Y. Goswami, Analysis of an innovative desalination system using low-grade solar heat, Desalination, 156(1–3) (2003) 323–332.
[17] N.H.A. Rahim, Utilisation of new technique to improve the efficiency of horizontal solar desalination still, Desalination, 138(1–3) (2001) 121–128.
[18] M. Boukar and A. Harim, Development and testing of a vertical solar still, Desalination, 158(1–3) (2003) 179.
[19] M.S. Abu-Jabal, I. Kamiya and Y. Narasaki, Proving test for a solar-powered desalination system in Gaza-Palestine, Desalination, 137(1– 3) (2001) 1–6.
[20] K. Schwarzer, M.E. Vieira, C. Faber and C. Müller, Solar thermal desalination system with heat recovery, Desalination, 137(1–3) (2001) 23–29.
[21] K. Voropoulos, E. Mathioulakis and V. Bellessiotis, Experimental investigation of a solar still coupled with solar collectors, Desalination, 138(1–3) (2001) , 103–110.

[22] A.A. Badran, A.A. Al-Hallaq, I.A.E. Salman and M.Z. Odat, A solar still augmented with a flat-plate collector, Desalination, 172(3) (2005) 227–234.
[23] J. de Koning and S. Thiesen, Aqua Solaris – an optimized small scale desalination system with 40 litres output per square meter based upon solar-thermal distillation, Desalination, 182(1–3) (2005) 503–509.
[24] K. Voropoulos, E. Mathioulakis and V. Bellessiotis, Solar stills coupled with solar collectors and storage tank – analytical simulation and experimental validation of energy behavior, Sol. Energy, 75(3) (2003) 199–205.
[25] L. García-Rodríguez, Renewable energy applications in desalination: state of the art, Sol. Energy, 75(5) (2003) 381–393.